xxx (xxxx) xxx

Contents lists available at ScienceDirect

Mucosal Immunology

journal homepage: www.elsevier.com/mi

Article

Distinct olfactory mucosal macrophage populations mediate neuronal maintenance and pathogen defense

Sebastian A. Wellford [a,b], Ching-Wen Chen [a], Marko Vukovic [d,e,f,g], Kristen A. Batich [a,c], Elliot Lin [a], Alex K. Shalek [d,e,f,g,h], Jose Ordovas-Montanes [d,e,i,j,k], Annie Park Moseman [a], E. Ashley Moseman [a,*]

[a] Department of Integrative Immunobiology, Duke University School of Medicine, Durham, NC, United States
[b] Cell Signaling and Immunity Section, Laboratory of Immune System Biology, National Institute of Allergy and Infectious Diseases, National Institutes of Health, Bethesda, MD, United States
[c] Department of Neurosurgery, Duke University School of Medicine, Durham, NC, United States
[d] Broad Institute of MIT and Harvard, Cambridge, MA, United States
[e] Ragon Institute of MGH, MIT and Harvard, Cambridge, MA, United States
[f] Institute for Medical Engineering and Science (IMES), MIT, Cambridge, MA, United States
[g] Department of Chemistry, MIT, Cambridge, MA, USA
[h] Institute for Integrative Cancer Research, Massachusetts Institute of Technology, Cambridge, MA, United States
[i] Division of Gastroenterology, Hepatology, and Nutrition, Boston Children's Hospital, Boston, MA, United States
[j] Harvard Stem Cell Institute, Cambridge, MA, United States
[k] Program in Immunology, Harvard Medical School, Boston, MA, United States

A B S T R A C T

The olfactory mucosa is important for both the sense of smell and as a mucosal immune barrier to the upper airway and brain. However, little is known about how the immune system mediates the conflicting goals of neuronal maintenance and inflammation in this tissue. A number of immune cell populations reside within the olfactory mucosa and yet we have little understanding of how these resident olfactory immune cells functionally interact with the chemosensory environment. Identifying these interactions will allow therapeutic manipulations that treat disorders such as post-viral olfactory dysfunction. Macrophages are the most prevalent immune cell type in the uninflamed olfactory mucosa and here, we identify two distinct tissue macrophage populations in murine olfactory mucosa. P2ry12^{hi} macrophages are transcriptionally specialized for neuron interactions, closely associated with olfactory neuron cell bodies, long-term tissue residents, and functionally specialized to phagocytose cells and debris, including olfactory neurons. Conversely, MHC Class II^{hi} macrophages are transcriptionally dedicated to cytokine production and antigen presentation, localized primarily within the olfactory lamina propria, more rapidly replaced by blood monocytes, and rapidly produce chemokines in response to viral infection. We further show that these macrophage signatures are present in human olfactory biopsies, and P2ry12-like olfactory macrophages are reduced in patients with long-term smell loss following COVID-19. Together, these data show that two olfactory macrophage populations regulate neurons and initiate the immune response, contributing to our understanding of both olfactory immunity and tissue-resident macrophage biology.

Introduction

Macrophages reside in tissues throughout the body, where they facilitate a plethora of functions both in homeostasis and disease[1–4]. Tissue macrophages contribute to inflammation in several ways, including cytokine and chemokine production, antigen presentation and lymphocyte activation, and effector molecule secretion to clear pathogens. On the other hand, macrophages can produce anti-inflammatory molecules, phagocytose dead cells and debris, and orchestrate tissue regeneration to promote wound healing. This dichotomy between pro- and anti-inflammatory properties of macrophages was originally described with the M1/M2 paradigm, but it is now appreciated that macrophages are far more diverse in their origin and functions[5,6]. Defining the heterogeneous properties of these cells will help us manipulate them to treat disease.

Macrophages within neuronal tissues have drawn attention for their ability to support and regulate neurological functions. Microglia are the resident macrophages within the central nervous system (CNS) and have been extensively studied for their contributions to neuronal function and neurodegenerative disease[7–9]. In addition to microglia, several macrophage populations have been described at brain borders[10–13], where these border-associated macrophages can defend against neurotropic

* Corresponding author.
E-mail address: ashley.moseman@duke.edu (E. Ashley Moseman).

https://doi.org/10.1016/j.mucimm.2024.07.009
Received 9 May 2024; Accepted 26 July 2024
Available online 27 July 2024
1933-0219/© 2024 The Author(s). Published by Elsevier Inc. on behalf of Society for Mucosal Immunology. This is an open access article under the CC BY-NC-ND license (http://creativecommons.org/licenses/by-nc-nd/4.0/).

pathogens[14,15]. Outside of the CNS, nerve-associated macrophages have been described in several tissues[16–18]. These populations exist in close conjunction with peripheral nerves and resemble microglia in some of their properties[19,20]. Like CNS macrophages, peripheral nerve macrophages must also balance the inflammatory response to infection with their duties to support neurons, and specialized subsets of nerve-associated macrophages may exist for these functions[21].

While tissue-resident macrophage populations have been separately characterized at several brain borders and mucosal tissues, macrophages within the olfactory mucosa, a tissue that straddles both neurological and mucosal functions, remain understudied. The olfactory mucosa (OM) is a densely innervated tissue that serves as a mucosal barrier for the upper airway and brain. At the OM surface, olfactory sensory neurons (OSNs) project their dendrites into the airway to detect odorant molecules, then rapidly relay sensory information through axon tracks directly into the olfactory bulb (OB) of the brain[22]. While this single-cell connection to the CNS efficiently accomplishes the sense of smell, olfactotropic pathogens also exploit this pathway to infect the brain while bypassing conventional CNS barriers[23–25]. Similarly, respiratory pathogens may use the olfactory mucosa as a foothold to spread to other tissues or individuals[24,25]. The OM itself can also become damaged by olfactotropic infection, as indicated by the widespread incidence of short and long-term post-viral olfactory dysfunction following diseases such as COVID-19[26–29]. Unlike most adult neuronal subtypes, OSNs can be replaced throughout life, especially following inflammation, and proper OSN regeneration from their local stem cell progenitors is required to preserve life-long olfaction[30]. Immune cells within the OM must therefore perform two tasks: supporting the fundamental olfactory process while simultaneously preventing olfactory pathogens from hijacking the olfactory tract to access the brain, disseminating within the respiratory tract, or directly damaging the OM.

As both important coordinators of the innate immune response and regulators of neuronal maintenance, macrophages are poised to play an important role in olfactory homeostasis and disease. Macrophages have been identified in human and animal OM[31,32] in association with OSN cell bodies and nerve fascicles[33]. OM macrophages have primarily been studied in response to chemical or surgical OSN ablation, where macrophage depletion has been shown to impair neurogenesis and expression of immune response genes[34]. Expression of macrophage effector cytokines[35,36], perhaps in response to OSN death[37–39], may be important for proper tissue regeneration. On the other hand, OM macrophages are the first responders to many respiratory and neurotropic pathogens[40–42]. However, if not properly regulated, this response can contribute to chronic inflammation that perpetuates smell loss[43]. It is unclear how OM macrophages balance their functions to support potentially contradictory goals in maintaining olfactory neurogenesis and robust immune defense, particularly in response to infection. This raises the possibility that distinct populations of olfactory macrophages mediate these divergent tasks. Understanding macrophage diversity and function within OM may support the design of therapeutics for anosmia and post-viral olfactory dysfunction. Moreover, defining olfactory macrophage functions, is an important step toward understanding the innate response to respiratory and neuroinvasive pathogens. Olfactory macrophage characterization will also broaden our understanding of macrophage diversity within tissues, especially their roles in neuroimmunity and defense at CNS borders.

In this study, we identify two distinct macrophage populations in the olfactory mucosa. Single-cell RNA sequencing demonstrates transcriptional differences between these subsets, which we term P2ry12^{hi} and MHC Class II^{hi}. Using these markers, we describe differences in tissue residency, localization, and morphology. We show that P2ry12^{hi} macrophages are functionally superior at neuron phagocytosis, while MHC Class II^{hi} macrophages are the major chemokine producers shortly after viral infection. Furthermore, we analyzed human olfactory biopsy data to find that macrophage populations are dysregulated in the context of post-COVID-19 smell loss. These results shed new light on how macrophage diversity contributes to olfactory maintenance and immunity as well as expand the literature on nerve-associated macrophages in health and disease.

Results

Two transcriptionally distinct olfactory macrophage populations

The olfactory mucosa is defined by the presence of olfactory sensory neurons (OSNs) and dominates most of the nasal mucosa space in mice (Fig. 1a). The mucosal tissue rests on bony turbinate structures and contains numerous parenchymal and hematopoietic cells[24]. While immune cells in the nasal mucosa have been previously described[44], the CD45^{+} cells within the olfactory mucosa specifically, have not been comprehensively surveyed, despite the tissue's importance as an upper airway and CNS barrier. Confocal imaging the OM from Cx3cr1-GFP mice, in which monocyte-macrophage lineage cells are fluorescently labeled, revealed numerous myeloid cells distributed throughout the tissue (Fig. 1b, c). Staining with F4/80, a widely conserved macrophage marker, indicated that the vast majority of these cells were macrophages (Supplementary Fig. S1a). These data are consistent with previous work that characterized Cx3cr1 in olfactory macrophage morphology[45–47]. Interestingly, we observed that the morphology of these cells varied widely across the tissue (Fig. 1c), ranging from stellate/glial-like to elongated to round. Macrophage shape heterogeneity within the neuroepithelium, basal lamina, and lamina propria led us to postulate that distinct macrophage subsets exist within the OM.

To systematically assess the resident immune cell heterogeneity in the OM, including macrophages, we performed single-cell RNAseq (scRNAseq) of CD45^{+} cells from murine OM. We sequenced samples both from naïve mice and from mice 40 days after infection with neurotropic vesicular stomatitis virus (VSV)[48] to capture the diversity of immune populations both before and after infection (Supplementary Fig. S1b). Processing mouse OM involved mincing the bony olfactory turbinates, leading to contamination from bone marrow hematopoietic cells. Previous studies of OM immune cells struggled to differentiate true olfactory cells from bone marrow[44,49,50]. To counteract this bone marrow contamination, we sequenced a sample of OM CD45^{+} CD19^{-} Ly6G^{-} cells to deplete B cell and neutrophilic bone marrow precursor cells and enrich for the rarer olfactory immune populations. Furthermore, we simultaneously sequenced samples from femoral bone marrow. By integrating these samples, we could cluster OM and BM CD45^{+} cells and subtractively determine the cells uniquely present in OM samples (Supplementary Fig. S1b). By removing clusters enriched for BM cells, we were left with a population of generally OM-specific immune cells (Fig. 1d) that encompassed data before and after infection, while including some less frequent olfactory immune populations.

Analysis of these OM CD45 + cells showed the existence of macrophages, dendritic cells, and γδ-T cells in naïve mice (Fig. 1d; Supplementary Table S1). Interestingly, nearest-neighbor clustering identified two olfactory macrophages populations present both before and after infection. Both macrophage populations expressed high levels of canonical macrophage genes, including *Cx3cr1*, *Ms4a7*, and *CD68* (Supplementary Fig. S1c-d, Supplementary Table S1). Differentially expressed genes between these macrophage populations included *P2ry12*, *Mrc1,* and *Pf4* in one cluster and *H2* genes, *Cxcl16*, and *Slamf7* in the other (Fig. 1e, Supplementary Table S1). Of note, the P2ry12^{hi} cluster also expressed high levels of Trem2 and Fcrls, which may correspond to a Trem2^{+} Fcrls^{+} population present in publicly available scRNAseq of the nasal mucosa[44]. We therefore termed these populations P2ry12^{hi} and MHC Class II^{hi} macrophages. *P2ry12* is a purinergic receptor that is a commonly used marker for microglia[4,8], while MHC Class II expression in macrophages is associated with canonical antigen presenting functions that regulate inflammation and defense. In naïve mice, P2ry12^{hi} macrophages outnumbered MHC Class II^{hi} macrophages (Fig. 1f,g, Supplementary Fig. S1d, Supplementary Table S1), but in

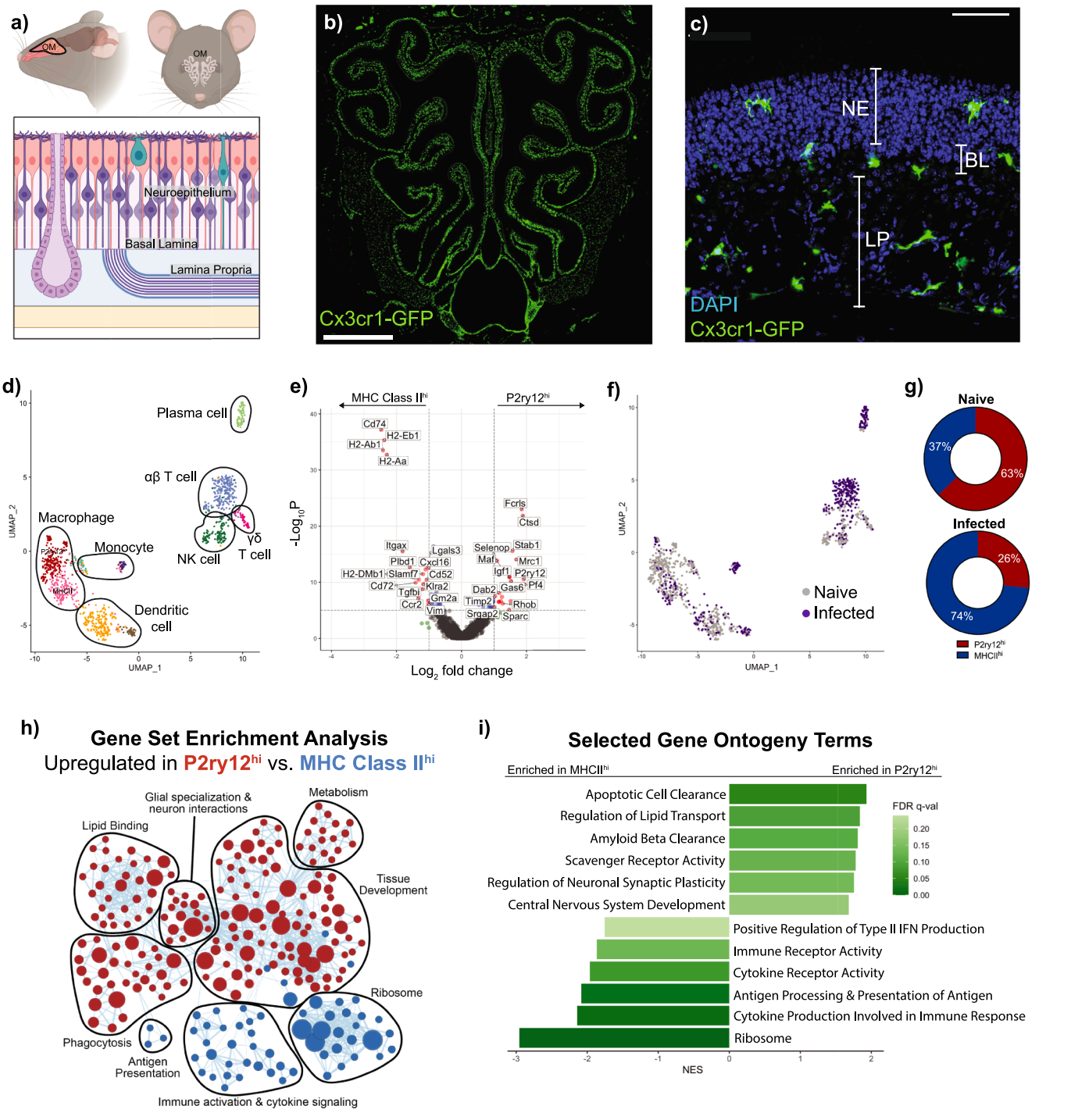


Fig. 1. Macrophage heterogeneity in the olfactory mucosa **a)** Diagram of murine olfactory mucosa. Top left: sagittal view of upper airway. Top right: coronal view of upper airway. Below: Diagram of cells in the olfactory mucosa, with olfactory sensory neurons shown in purple. Neuroepithelium, basal lamina, and lamina propria portions of the tissue are labeled. **b)** Coronal section of olfactory mucosa from Cx3cr1-GFP mouse. Green = Cx3cr1-GFP. Scale bar: 1000 μm. **c)** Cx3cr1-GFP olfactory mucosa, with neuro-epithelium (NE), basal lamina (BL), and lamina propria (LP) labeled. Green = Cx3cr1-GFP, Blue = DAPI. Scale bar: 50 μm. **d)** UMAP projection of scRNAseq data from $CD45^{+}$ olfactory mucosa cells, containing cells from naïve mice and mice 45 days-post VSV infection. **e)** Volcano plot comparing differentially expressed genes between two macrophage subsets ($P2ry12^{hi}$ and MHC Class II^{hi}). **f)** UMAP projection of data in (D) with cells from naïve mice in gray and mice previously infected with VSV (45 dpi) in orange. **g)** Quantification of (**f**), displaying the proportion of macrophages in either naïve or previously infected mice that are either $P2ry12^{hi}$ or MHC Class II^{hi}. **h)** Gene set enrichment analysis between $P2ry12^{hi}$ (red) and MHC Class II^{hi} (blue) olfactory macrophages. GO terms illustrated in Cytoscape map and grouped by function. **i)** Selected gene ontogeny terms from (**h**) plotted by net enrichment score (NES) and FDR q-value. See also Supplementary Fig. S1. (For interpretation of the references to colour in this figure legend, the reader is referred to the web version of this article.)

mice previously infected with VSV, MHC Class II^{hi} macrophages composed a much larger proportion of olfactory macrophages, suggesting differential roles for these subsets in homeostasis and disease, perhaps based on expansion or immigration of blood-derived cells following infection. Additional changes in mice recovered from VSV infection included a decrease in γδ-T cells and an increase in αβ-T cells (predominately CD8^{+}) as well as class-switched plasma cells (primarily IgA^{+}) (Supplementary Fig. S1d, Supplementary Table S1). To further characterize the transcriptional differences between the two macrophage populations, we performed gene set enrichment analysis. Gene ontology (GO) terms that differed between these sets included pathways associated with phagocytosis, neuron interactions, and tissue development in P2ry12^{hi} macrophages and pathways related to immune activation, cytokine signaling, and antigen presentation in MHC Class II^{hi} macrophages (Fig. 1h-i, Supplementary Table S1). This analysis of single-cell transcriptomes suggested two distinct populations of olfactory macrophages, one poised for neuron maintenance (P2ry12^{hi}) and the other primed for inflammatory mediator production (MHC Class II^{hi}).

P2ry12^{hi} and MHC Class II^{hi} macrophages differ in tissue residency

Tissue macrophage populations differ in their ability to reside long-term within tissues[6]. Whether macrophage populations are long-term, self-renewing populations, or continuously replaced by circulating monocytes has been shown to indicate a variety of functional roles across health and disease[51], including in the nervous system[10,11,19,52]. We therefore tested whether these two olfactory macrophage populations were long-term self-renewing tissue residents or replaced by circulating cells.

Using flow cytometry on olfactory mucosal tissues[53], we could distinguish P2ry12^{hi} (CD45^{lo}, P2ry12^{hi}) and MHC Class II^{hi} macrophages (CD45^{hi}, P2ry12^{lo}) (Supplementary Fig. S2a, b). To analyze the OM macrophage tissue lifespans we employed a tamoxifen inducible pulse-chase system. By tamoxifen treating Cx3cr1$^{CreERT2\text{-}YFP}$ x LSL-tdTomato mice[54], olfactory macrophages, and any potential offspring were indelibly marked by a fluorescent tdTomato reporter. Over time, long-lived or self-renewing macrophages would remain tdTomato^{+}, while newly generated bone marrow-derived cells would be YFP^{+} tdTomato^{-} (Fig. 2a). We found that up to 20 weeks following tamoxifen treatment, olfactory macrophages, as a whole, experience an intermediate turnover rate compared to olfactory bulb microglia (within the CNS) and blood monocytes (Fig. 2b). However, when analyzed by subset, P2ry12^{hi} macrophages remained mostly tdTomato^{+}, indicating they were bona-fide tissue-resident cells (Fig. 2c). On the other hand, the majority of MHCII^{hi} macrophages experienced more rapid turnover, indicating that this population was continuously supplemented by circulating monocytes (Fig. 2c). These differences in tissue residency indicate that P2ry12^{hi} and MHCII^{hi} macrophages are distinct lineages of cells.

We next wondered whether P2ry12^{hi} macrophages would retain their self-renewing capacity even in the face of a harsh inflammatory challenge. We therefore performed the same tamoxifen labeling experiment but infected the Cx3cr1$^{CreERT2\text{-}YFP}$ x LSL-tdTomato mice with VSV 4 weeks after tamoxifen treatment. VSV robustly replicates within olfactory sensory neurons, leading to massive tissue damage and inflammatory infiltrate[48]. Following clearance, the olfactory mucosa is regenerated about 4–6 weeks after the initial challenge[55]. Similar to naïve mice, MHCII^{hi} macrophages were rapidly replaced by circulating cells following viral challenge (Fig. 2d). A large portion P2ry12^{hi} macrophages were also initially derived from circulation following VSV challenge, indicating that circulating cells could adopt a P2ry12^{hi} phenotype under some circumstances. But as time passed following viral-driven inflammation, the percentage of tdTomato^{+} P2ry12^{hi} macrophages again rose, indicating that P2ry12^{hi} macrophages were able to self-replenish their niche without contribution from circulating cells (Fig. 2d). This suggested that P2ry12^{hi} macrophages are a stable lineage that is not frequently replaced by circulating monocytes, even following intense inflammation.

P2ry12^{hi} and MHC Class II^{hi} macrophages localize to different tissue niches

Given the differences in P2ry12^{hi} and MHC Class II^{hi} olfactory macrophage gene expression and tissue residence, we sought to determine whether these macrophages fill distinct sub-tissue anatomical niches. The olfactory mucosa can be divided into distinct layers (Fig. 1a, c)[56]. The avascular neuroepithelium is directly adjacent to the nasal airway and contains the cell bodies of olfactory sensory neurons. Beneath this is the basal lamina, where stem cells reside that regenerate the apical epithelial cells. Underneath this structure lies the vascularized

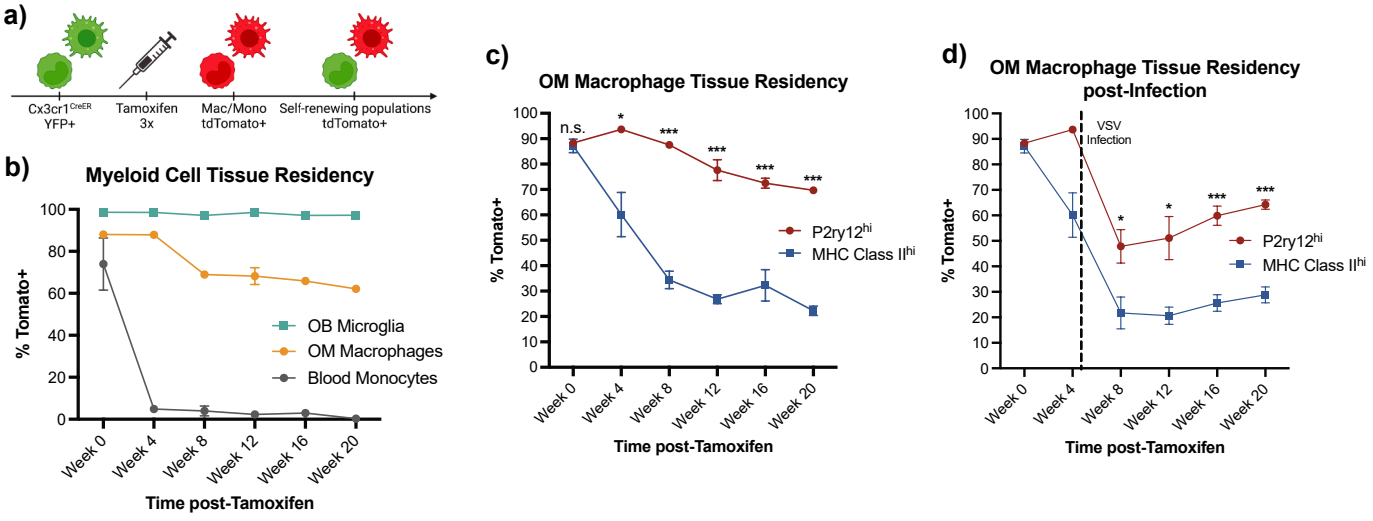


Fig. 2. Tissue residency of P2ry12^{hi} and MHC Class II^{hi} olfactory macrophages **a)** Schematic depicting experiments in (**b**)–(**d**). Cx3cr1-CreER^{YFP} x LSL-tdTomato mice were injected with tamoxifen, and the percentage of tdTomato^{+} olfactory macrophages were quantified at subsequent timepoints. Four mice were measured at each timepoint in (B-D). **b)** The frequency of tdTomato^{+} olfactory bulb (OB) microglia, olfactory mucosa (OM) macrophages, and blood monocytes were measured at each timepoint. **c)** Olfactory macrophages from (**b**) were further gated into P2ry12^{hi} and MHC Class II^{hi} subsets. **d)** As in **c**), olfactory macrophage subsets were quantified for the percent of tdTomato^{+} cells, but 28 days following tamoxifen treatment, mice were infected intranasally with VSV. n.s. = not significant, p* < 0.05, p** < 0.01, p*** < 0.001. See also Supplementary Fig. 2.

lamina propria, which contains a heterogeneous mixture of cell types and structures including olfactory sensory neuron axon tracts, fibroblasts, Bowman's glands, and endothelial vessels, among others (Fig. 1a, c). In each region, macrophages may be mediating specific interactions with each cell type, so we sought to spatially define the macrophage phenotypes within these anatomical compartments.

MHC Class II expression was used to histologically classify these OM macrophage subsets in Cx3cr1$^{CreERT2\text{-}YFP}$ x LSL-tdTomato mice via fluorescent antibody staining of fixed frozen tissue sections (Fig. 3a–d). MHC Class II^{hi} macrophages made up a majority of macrophages within the lamina propria and along the basal lamina (Fig. 3e). However, within the neuroepithelium, MHC Class II^{hi} macrophages were rarely observed (Fig. 3e). MHC Class II expression was increased across all tissue compartments as the mice aged (Fig. 3f), perhaps reflecting the inflammatory influence of environmental microbe exposure. To determine if long-term residency varied by tissue compartment, we also quantified the differential abundance of long-term resident tdTomato^{+} macrophages. Twenty weeks post-tamoxifen treatment, tdTomato^{+} macrophages still made up a vast majority of macrophages in the neuroepithelium and proportionally fewer cells in the lamina propria (Fig. 3g). Combined, these data suggest that P2ry12^{hi} macrophages more frequently localize to the neuroepithelium, while MHC Class II^{hi} macrophages localize to the lamina propria, although P2ry12^{hi} macrophages can be found within the lamina propria as well. Over time, the lamina propria undergoes more rapid replacement from peripheral cells, and MHC Class II expression is increased in macrophage populations throughout the tissue.

Form often follows function, and tissue macrophage heterogeneity is associated with a variety of characteristic shapes, including round alveolar macrophages, stellate Kupffer cells, ramified microglia, or flattened wound-associated macrophages[57–59]. Indeed, whole mount imaging of olfactory mucosa "peels" taken from the septum as previously described[60], revealed significant variation in OM macrophage morphology in Cx3cr1-GFP mice, particularly between macrophages in

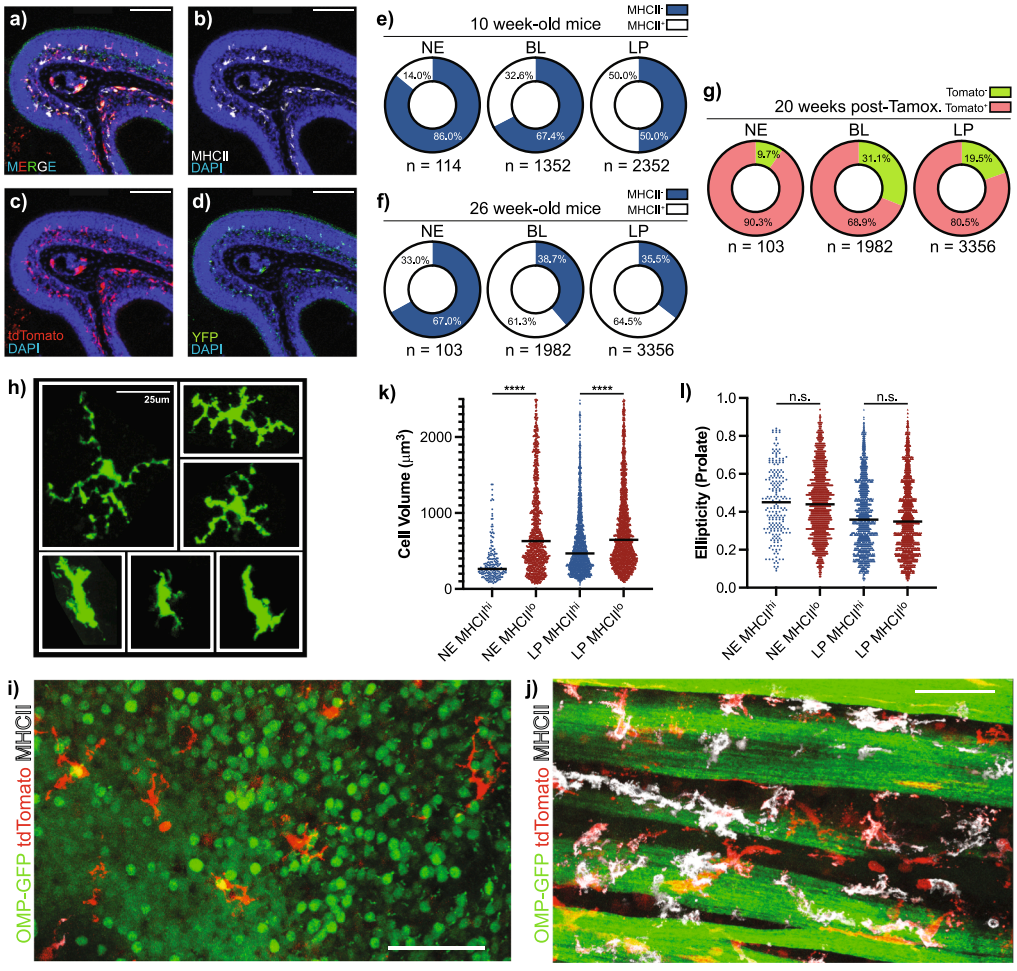


Fig. 3. P2ry12^{hi} and MHC Class II^{hi} macrophages differ in localization and morphology **a and d)** Cx3cr1-CreER^{YFP} x LSL-tdTomato olfactory mucosa coronal section from mouse 20 weeks post-Tamoxifen treatment. Merge in (**a**), DAPI=blue, MHC Class II (IA/IE) = white (**b**), tdTomato = red (**c**), YFP=green (**d**). Scale bars = 100 μm. **e–f)** Quantification of MHC Class II^{+} and MHC Class II^{-} macrophages from olfactory mucosa sections of Cx3cr1-CreER^{YFP} x LSL-tdTomato mice. Six sections from three 10 week-old mice were quantified in (**e**). Eight sections from four 26 week-old mice were quantified in (**f**). NE=Neuroepithelium, BL=Basal lamina, LP=Lamina propria. **g)** Percentage of tdTomato^{+} and tdTomato^{-} YFP^{+} cells from mice in (**f**), 20 weeks post-Tamoxifen treatment. NE=Neuroepithelium, BL=Basal lamina, LP=Lamina propria. **h)** Representative whole mount images of Cx3cr1-GFP olfactory macrophages with differing morphologies; upper 3 panels are MHC Class II^{-} cells from apical neuroepithelium, and lower panels are MHC Class II^{+} cells from the lamina propria. Scale bar = 25 μm. **I and j)** Whole mount images of Cx3cr1-CreER^{YFP} x LSL-tdTomato x OMP-GFP olfactory mucosa 3 days post-Tamoxifen treatment. Neuroepithelium shown in **h**, lamina propria shown in **i**. GFP=green, tdTomato (macrophages) = red, MHC Class II=white. Scale bars = 50 μm. **K and l)** Quantification of whole mount olfactory mucosa tissues from five Cx3cr1-CreER^{YFP} x LSL-tdTomato x OMP-GFP mice. Surfaces were constructed in Imaris for macrophages based on tdTomato and MHC Class II expression to measure macrophage volume (**k**) and macrophage prolate ellipticity (**l**). Data were quantified by region of the tissue, with macrophages near OSN cell bodies defined as neuroepithelial (NE) and macrophages near OSN axon tracks defined as within the lamina propria (LP). Statistical significance determined using Kolmogorov-Smirnov *t*-test in **k-l**. n.s. = not significant, p**** < 0.0001. (For interpretation of the references to colour in this figure legend, the reader is referred to the web version of this article.)

the apical neuroepithelium (Fig. 3h, upper panels) and those in the lamina propria (Fig. 3h, lower panels). To gain insight into how olfactory macrophage shapes and functions differ, we sought to quantify morphological diversity across macrophage subsets and anatomical tissue niches (Fig. 1a, c). Confocal imaging of whole mounted olfactory mucosa "peels" allowed olfactory macrophage analysis *in situ* without subjecting individual cells to sectioning. Cx3cr1$^{CreERT2\text{-}YFP}$ x LSL-tdTomato mice were crossed with OMP-GFP reporter mice[61], in which olfactory sensory neurons specifically express GFP, enabling simultaneous visualization of macrophages (red) and olfactory sensory neurons (green) (Fig. 3i-j). After tamoxifen treatment and antibody staining for MHC Class II, the cell volume and cell shape of MHC Class II^{hi} and MHC Class II^{lo} cells were measured within the neuroepithelium (near OSN cell bodies, Fig. 3i) and the lamina propria (near OSN axon tracks, Fig. 3j).

With a more extended glial-like shape with thin membrane processes, MHC Class II^{lo} macrophages appear grossly larger than MHC Class II^{hi} macrophages (Fig. 3i–k), This size difference was reflected by a significant volumetric difference in both the neuroepithelium and the lamina propria (Fig. 3k). We also quantified the prolate ellipticity of olfactory macrophages, an elongation measurement associated with a wound-healing phenotype[62]. Within the neuroepithelium or the lamina propria, we did not observe differences between the two macrophage subsets. However, cells within the neuroepithelium had higher prolate ellipticity than cells within the lamina propria (Fig. 3l) regardless of MHC Class II expression. These data suggest that the sub-anatomical location governs olfactory macrophages morphology that likely plays a role in site-specific functions[59].

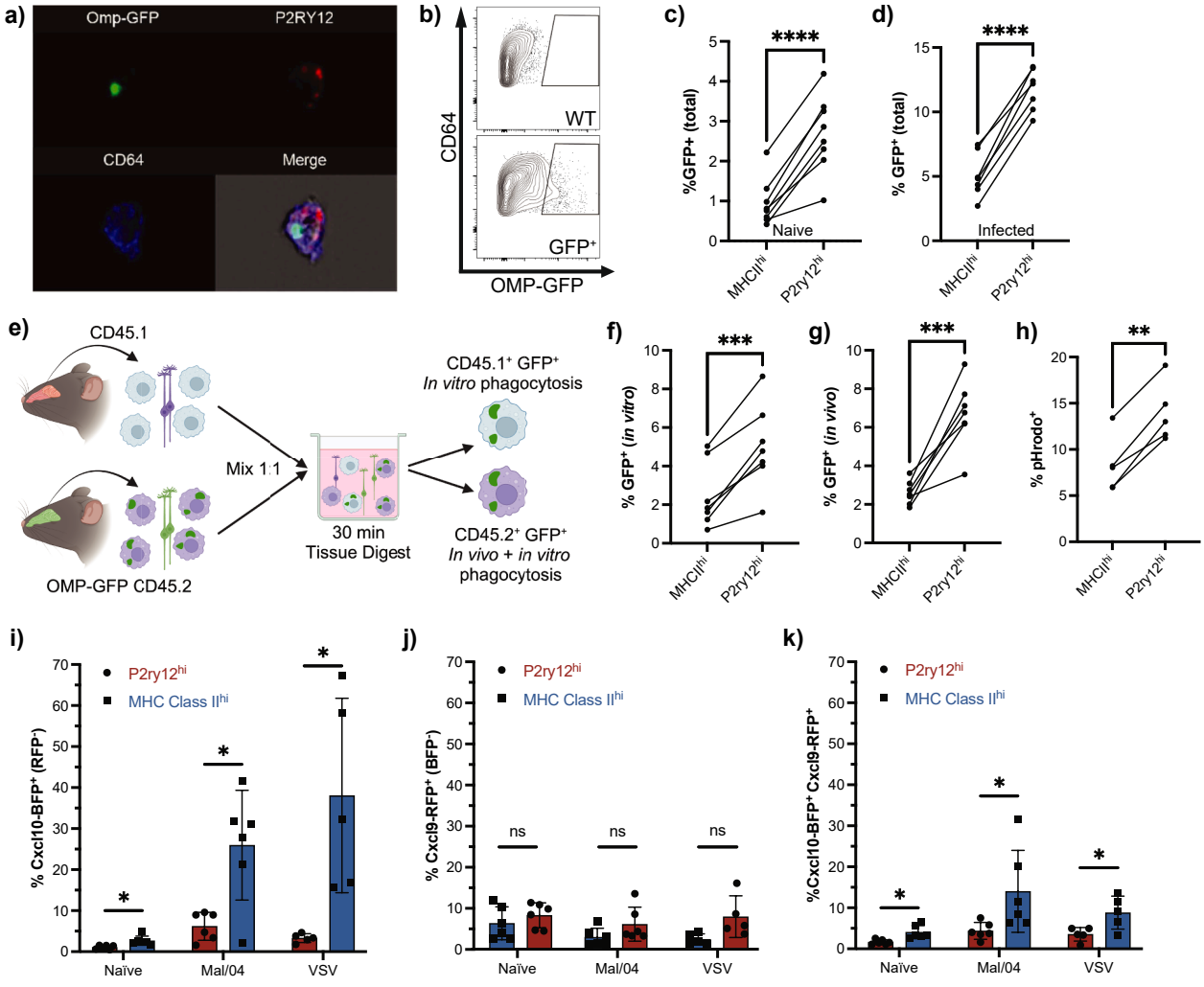


Fig. 4. P2ry12^{hi} macrophages phagocytose olfactory neurons while MHC Class II^{hi} produce chemokines early after infection **a)** Imaging cytometer visualization of a macrophage (CD64^{+}, P2ry12^{+}) internalizing GFP signal from an OMP-GFP mouse. **b)** OMP-GFP internalization by macrophages is quantifiable via conventional flow cytometry. Gated on CD45^{+} CD45.2-IN^{+} CD11b^{+} F4/80^{+} CD64^{+}. **C and d)** Comparison of OMP-GFP internalization between P2ry12^{hi} and MHC Class II^{hi} olfactory macrophages in naïve mice (**c**) and mice 24 h after Mal/04 Influenza B infection (**d**). **e–g)** Quantification of *in vitro* and *in vivo* macrophage phagocytosis. CD45.1^{+} WT mouse OM was mixed with CD45.2^{+} OMP-GFP OM during tissue digest (**e**). CD45.1^{+} macrophage internalization of OMP-GFP was used to calculate *in vitro* OSN phagocytosis (**f**). This rate was subtracted from the amount of CD45.2^{+} macrophage OMP-GFP internalization to calculate *in vivo* OSN phagocytosis (**g**). **h)** OM cells were mixed with fluorescent red pHrodo *E. coli* bioparticles, and the frequency of macrophage pHrodo red internalization was calculated. **i–k)** Macrophage subset expression of Cxcl9 and Cxcl10 quantified from REX3 (Cxcl9^{RFP}/Cxcl10^{BFP}) reporter mice, either naïve or 24 h post-infection with Influenza B Mal/04 or VSV. Frequency of Cxcl10^{+}Cxcl9^{-} macrophages (**i**), Cxcl10^{-}Cxcl9^{+} macrophages (**j**), and Cxcl10^{+}Cxcl9^{+} macrophages (**k**) quantified and compared between P2ry12^{hi} and MHC Class II^{hi} subsets. For **c,d,f,g, and h**, lines between points connect populations from the same animal. Statistical significance determined with ratio paired *t*-test in (**c and d, f–h**) and parametric *t*-test with Welch's correction in (**i–k**). Data are pooled from two independent experiments, n = 5–8. ns = not significant, p* < 0.05, p** < 0.01, p*** < 0.001, p**** < 0.0001. See also Supplementary Fig. S3. (For interpretation of the references to colour in this figure legend, the reader is referred to the web version of this article.)

P2ry12^{hi} macrophages phagocytose olfactory neurons while MHC Class II^{hi} produce chemokines early after infection

Since P2ry12^{hi} macrophages expressed genes associated with neuronal maintenance and phagocytosis, while MHC Class II^{hi} macrophages had a transcriptional profile associated with cytokine secretion and inflammation, we sought to determine whether these cells performed distinct functions in response to infection. Using imaging cytometry of OMP-GFP mice, we were able to visualize macrophage phagocytosis of olfactory sensory neuron fragments (Fig. 4a). Furthermore, this GFP engulfment could be quantified with conventional flow cytometry (Fig. 4b). When olfactory neuron GFP phagocytosis was quantified by macrophage subset, P2ry12^{hi} macrophages were shown to be superior at internalizing GFP compared with MHC Class II^{hi} macrophages (Fig. 4c). When mice were infected with an olfactotropic influenza B virus (Mal/04)[63], the rates of phagocytosis were increased, with P2ry12^{hi} macrophages still engulfing olfactory neuron fragments at a higher frequency than MHC Class II^{hi} macrophages (Fig. 4d).

This macrophage phagocytosis of neuronal GFP signal could either result from *in vivo* phagocytosis or be a product of macrophage-neuron interactions during the tissue digestion required to generate single-cell suspensions. Furthermore, we desired to determine whether P2ry12^{hi} macrophages were intrinsically better at phagocytosing OSN fragments, or if this was merely because they reside in closer proximity to OSNs *in situ*. To assess whether our observed phagocytosis was occurring *in vivo* or *in vitro*, we co-digested our olfactory mucosa tissue from CD45.2^{+} OMP-GFP mice with olfactory mucosa tissue from WT CD45.1^{+} mice, both 24 h after Mal/04 infection (Fig. 4e). Using this approach GFP can only be acquired by CD45.1^{+} macrophages through *in vitro* phagocytosis. Indeed, we observed that CD45.1^{+} macrophages could in fact internalize some GFP signal during the *in vitro* co-incubation (Fig. 4f). While this rate was lower than the overall CD45.2^{+} (endogenous) phagocytosis rate, all P2ry12^{hi} macrophages internalized OSN fragments more frequently, indicating that they are superior at phagocytosing olfactory neurons independent of their tissue localization (Fig. 4f). To estimate the rate of *in vivo* phagocytosis, we subtracted the CD45.1^{+} macrophage *in vitro* GFP internalization frequency from the CD45.2^{+} macrophage population. P2ry12^{hi} macrophages were still found to more frequently internalize GFP signal *in vivo* (Fig. 4g), indicating that this process occurs within living animals. Lastly, we investigated whether the ability of P2ry12^{hi} macrophages to efficiently phagocytose neuron fragments was a property specific to interactions with neuronal cells, or a more general indicator of phagocytic capacity. We therefore incubated olfactory mucosa cells *in vitro* with fluorescent pHrodo *E. coli* bioparticles (Fig. 4h, Supplementary Fig. S3a). P2ry12^{hi} macrophages more frequently phagocytosed these bioparticles compared with MHC Class II^{hii} macrophages, suggesting that P2ry12^{hi} macrophages are generally more primed for phagocytic function.

In addition to phagocytosis, macrophages are some of the first cells to produce inflammatory cytokines and chemokines following an infection. Consistent with this, MHC Class II^{hi} olfactory macrophages expressed many inflammatory genes. To test whether these two macrophage populations differentially produced chemokines in response to infection, we infected Cxcl9^{RFP}Cxcl10^{BFP} (REX3) mice[64] with influenza B Mal/04 or with VSV (Supplementary Fig. S3b). Cxcl10 and Cxcl9 are canonically stimulated by Type I and Type II interferons (IFNs), respectively[65]. At baseline prior to infection, MHC Class II^{hi} macrophages expressed more *Cxcl10* than P2ry12^{hi} macrophages (Fig. 4i-k). Accordingly, 24 h following infection with either virus, the frequency of MHC Class II^{hi} macrophages expressing *Cxcl10* dramatically increased, while the frequency of *Cxcl10* expression by P2ry12^{hi} remained low (Fig. 4i). While neither population contained many cells that produced *Cxcl9* only (Fig. 4j), a larger portion of MHC Class II^{hi} macrophages produced both *Cxcl9* and *Cxcl10* simultaneously (Fig. 4k). These results indicate that MHC Class II^{hi} macrophages quickly respond to olfactory infection, possibly via Type I IFN, while P2ry12^{hi} macrophages do not produce chemokines in the presence of virus. The *Ifnar1/2* and *Ifngr1/2* genes are not differentially expressed between these macrophage subsets (Table S1), suggesting that this response may be regulated by dissimilarities in chromatin accessibility or intracellular signaling pathways. This is consistent with our scRNAseq results that indicated MHC Class II^{hi} macrophages are enriched in genes related to cytokine receptor signaling and interferon pathway regulation (Fig. 1e, i).

A human olfactory macrophage subset associated with post-COVID olfactory dysfunction

The human olfactory mucosa (Fig. 5a) is frequently the target of respiratory and neurotropic pathogens. SARS-CoV-2 directly infects ACE2^{+} sustentacular cells in the olfactory mucosa[25], often leading to both short- and long-term smell loss (hyposmia). The immune response contributes to both pathogen clearance in the upper airway and to olfactory tissue regeneration[24]. Since we identified functionally distinct populations of murine olfactory macrophages, we sought to assess human olfactory macrophage heterogeneity, both at homeostasis and following infection to identify contributions to long-term olfactory deficits. We therefore reanalyzed previously published scRNAseq data from human olfactory biopsies[66]. These samples included olfactory mucosa from normosmic patients, hyposmic patients, and patients with hyposmia long-term after COVID-19. Nearest-neighbor macrophage clustering identified several macrophage populations present across all patient groups (Fig. 5b, Supplementary Table S2). To compare these clusters to our murine macrophages, we created a gene set for genes enriched in our P2ry12^{hi} macrophage population (Supplementary Tables S1, S2). This gene set was highly enriched in the "cluster 4" human macrophages (Fig. 5c). The "P2ry12"-like cluster 4 was enriched for several genes associated with macrophage-neuron interactions, phagocytosis, and tissue regeneration (Supplementary Fig. S4a, Supplementary Table S2). Interestingly, while this population composed a large portion of macrophages in normosmic control patients, it was decreased in hyposmic patients and further diminished in post-COVID hyposmic patients (Fig. 5d, e). While it is unclear if this reduced cluster 4 macrophage frequency reflected a reduction in their number or an increase in other macrophage populations, it may represent an imbalance of inflammatory and regenerative macrophages in these disease states. We conducted gene set overlap analysis to further analyze the macrophage populations in post-COVID hyposmic patients and found that they shared gene sets exclusively with murine MHC Class II^{hi} macrophages, but not murine P2ry12^{hi} macrophages (Fig. 5f, Supplementary Fig. S4b, Supplementary Table S2). On the other hand, patients who did not have prior COVID infection shared substantial gene set overlap with murine P2ry12^{hi} macrophages (Fig. 5f, Supplementary Table S2). These results indicate that P2ry12^{hi} and MHC Class II^{hi} olfactory macrophage signatures are present in humans and that reduction in P2ry12^{hi} macrophage frequency is associated with post-COVID smell loss.

Discussion

Macrophages vary across tissues in their residency time, morphology, and function. The olfactory macrophage subsets we identified, defined by P2ry12 and MHC Class II surface expression, align with the dual resident tissue macrophage populations found across many other tissues, and that are in part defined by MHC Class II expression[5]. In the lung, another airway barrier tissue, two interstitial macrophages populations (CD206^{hi}Lyve1^{hi}MHCII^{lo} and CD206^{loi}Lyve1^{lo}MHCII^{hi}) coexist with properties that mirror P2ry12^{hi} and MHC Class II^{hi} olfactory macrophages, respectively[67]. While *Lyve1* was not detected at high levels in our scRNAseq data, *Mrc1* (CD206) – an endocytic receptor- was one of the top genes expressed in P2ry12^{hi} compared to MHC Class II^{hi} olfactory macrophages (Table S1). Thus, our olfactory macrophages subsets may fit into the pan-tissue macrophage paradigm[5,67]. Moreover,

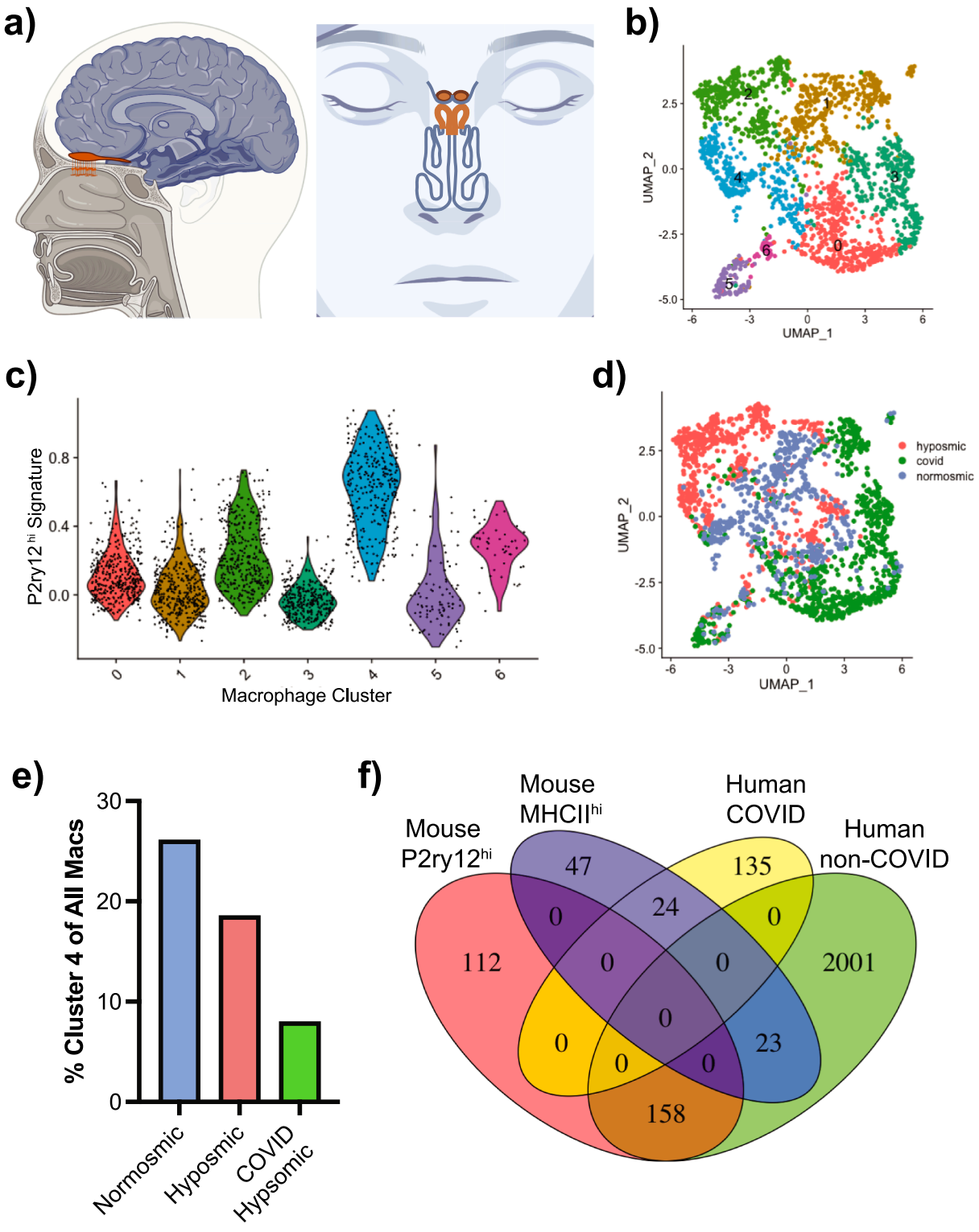


Fig. 5. A human olfactory "P2ry12"-like macrophage subset is diminished with post-COVID smell loss **a)** Diagram of human olfactory tissue. Left shows olfactory sensory neurons projecting into the olfactory bulb of the brain. Right shows olfactory regions on the upper turbinates of the nasal passages. **b–f)** Previously published scRNAseq data of human olfactory biopsies was reanalyzed to study macrophage populations. **b)** UMAP projection of human olfactory macrophage clusters. **c)** Violin plot showing enrichment scores for mouse P2ry12^{hi} macrophage signature. Clusters from human olfactory macrophages in (**b**). **d)** UMAP projection of human olfactory macrophages as in (b), separated by patient condition. Normosmic = patients with functional sense of smell, hyposmic = patients with a reduced sense of smell, COVID=patients previously infected with COVID who have not recovered the sense of smell. **e)** Frequency of macrophage Cluster 4 as a percentage of total macrophages for each patient condition. **f)** Gene set overlap analysis pathways shared between mouse P2ry12^{hi} olfactory macrophages, mouse MHC Class II^{hi} olfactory macrophages, human post-COVID olfactory macrophages, and human normosmic or hyposmic olfactory macrophages. See also Supplementary Fig. S4.

our results contribute to the growing appreciation of nerve-associated macrophages across tissues, and similar to other studies, show that functional heterogeneity exists within this compartment[12,21]. While OSNs are typically considered part of the peripheral nervous system, the olfactory nerve is continuous with the CNS; considering how P2ry12^{hi} macrophages resemble microglia in their gene signatures and some functions, could we consider this subset to be bona-fide microglia? While this possibility has not been directly addressed, we did not detect any expression of *Sall1*, a microglia-defining transcription factor[68], within our olfactory macrophages. Furthermore, our macrophages expressed high levels of *Pf4*, a gene expressed by brain border macrophages but not by microglia[69]. We posit that P2ry12^{hi} olfactory macrophages are similar to peripheral nerve resident macrophages, which have been shown to express a core gene signature similar to microglia, but remain distinct[20]. More detailed examination of olfactory macrophage ontogeny (including embryonic fate mapping) and direct comparison to nerve-associated macrophages will help define olfactory macrophages in relation to other tissue macrophage subsets. It is also possible that OM macrophages are more diverse than identified in this study; our scRNAseq contained a relatively small number of macrophages, and more targeted analysis could unveil more granularity within these populations.

Our data help resolve the conundrum of how olfactory macrophages balance the dual responsibilities of immune defense and neuronal maintenance. The OM has two distinct macrophages populations, one dedicated to each purpose. P2ry12^{hi} macrophages are specialized for neuron interactions; indeed, P2RY12 itself has been shown to be important for neuron protection[70]. We identified other gene signatures in the P2ry12^{hi} population that could hint at their role in OSN function, such as clearance of lipids and amyloid plaques[71], which have been implicated in olfaction and neurodegeneration[72,73]. P2ry12^{hi} macrophages also expressed gene sets associated with complement-mediated synaptic engulfment and synapse interactions[74,75], which may help OSNs guide their axons through the lamina propria and into the OB. The phagocytic ability of P2ry12^{hi} macrophages is also likely important for OSN function. Unlike most neurons, OSNs are homeostatically lost and replaced throughout life. This cellular turnover likely generates cellular debris and we demonstrated that P2ry12^{hi} macrophages are internalizing OSN fragments even at homeostasis. This internalization could represent either trogocytosis or the uptake of dead cells. Macrophage phagocytosis is also likely important during infection resolution and in tissue regeneration, as has been shown for microglia phagocytosis in neuroinflammation[76,77]. Indeed, several studies suggest macrophages are important for tissue regeneration following OSN death[34,37,47]. Macrophage interactions with olfactory stem cells may either contribute to or hinder this regenerative process, as has been observed with other immune cell populations in the OM[66,78]. Our group recently identified the blood-olfactory barrier (BOB)[79], and restrictive endothelial barrier in the OM comparable to the blood–brain barrier (BBB). Given the importance of microglia in BBB maintenance[80], could olfactory macrophages contribute to the formation or preservation of the BOB? P2ry12 coupling has been shown to be important for BBB structure[81], so P2ry12^{hi} macrophages may similarly regulate the BOB. Overall, these macrophages likely contribute to the process of olfaction, a conclusion supported by a previous study that demonstrated impaired sense of smell in CSF1R-deficient mice[82], although brain-resident cells could be responsible for this effect rather than OM macrophages.

MHC Class II^{hi} macrophages, rather than direct neuronal support, are predisposed to initiate the immune response and guard the OM from infection. Many allergens[50] and olfactotropic pathogens[24], neuroinvasive or otherwise, threaten the OM, and mounting an effective innate response can prevent dissemination to the brain or other tissues. Macrophages and microglia are vital for the response to several CNS infections[55,83,84], especially at brain borders. Indeed, in an interesting parallel, the MHC Class II^{hi} olfactory macrophages described here seem to resemble a population of MHCII^{+} macrophages in the meninges that guard against infection of the brain parenchyma[15,85]. In addition to antigen presentation, olfactory MHC Class II^{hi} macrophages rapidly upregulate *Cxcl10* suggesting they may help recruit T cells and other hematopoietic cells to the OM. Olfactory immunity has received increased attention in the wake of the COVID-19 pandemic, as smell loss is one of the most commonly reported symptoms[25]. The quality and magnitude of the innate response is critical for SARS-CoV-2 control[86], but at the same time, sustained inflammation can contribute to post-viral olfactory dysfunction in COVID-19[28,29] Indeed, recent work has shown a persistent IFNɣ signature in the olfactory tissue of COVID induced long-term hyposmic patients[87]. One mechanism by which macrophages may impair olfactory recovery could be inflammatory cross-talk with local olfactory stem cells, either directly or by continued recruitment or activation of circulating effector lymphocytes[43,66]. We observed that the frequency of MHC Class II^{hi} macrophages increased not only after infection, but these cells also accumulated with age, suggesting they may play a role in shaping the inflammatory environment that contributes to age-associated smell loss[78]. Overall, the delicate balance between neuronal support and inflammation in the OM must still be investigated in greater detail, but our identification of distinct P2ry12^{hi} and MHC Class II^{hi} macrophage subsets provides an important tentpole for our understanding of olfactory mucosa immunity.

Methods

Data and code availability

Single-cell RNA sequencing(scRNAseq) data and associated code are deposited on GitHub https://github.com/SebastianWellford/OlfactoryMucosa_Macrophages. An interactive ShinyApp of olfactory mucosa immune and stromal cells can be found at https://mosemanlab.shinyapps.io/olfactory_mucosa/.

scRNAseq and analysis

scRNAseq data was generated using the Seq-Well platform[88]. Four separate samples from OMP-GFP+mice were concatenated to comprehensively survey olfactory mucosa immune cells while minimizing contaminate from turbinate bone marrow. One contained OMP-GFP^{-} CD45^{+} cells, another contained OMP-GFP^{-} CD45^{+} Ly6g^{-} CD19^{-} cells, one contained OMP-GFP^{-} CD45^{+} Ly6g^{-} CD19^{-} cells from intranasally VSV infected mice (45 days post infection), and one contained bone marrow. Data analysis and processing was performed in RStudio using the Seurat v_4.1.0 analysis package and standard pre-processing workflow. Nearest-neighbor clustering was used to identify CD45^{+} cell populations. Clusters with a higher proportion of bone marrow sample cells than olfactory mucosa sample cells were then removed from the data to yield true "olfactory mucosa" immune cells. Gene set enrichment analysis was performed using GSEA v_4.0.3 and Cytoscape using gene sets obtained from Molecular Signatures Database m5.go.v2023.1.Mm.symbols.

Analysis of previously published scRNAseq data obtained from Finlay et. al.[66] was similarly analyzed in RStudio using Seurat v_4.1.0. Macrophages were subsetted from samples with validated olfactory tissue. The "P2ry12^{hi}" signature was created by selecting genes significantly upregulated in P2ry12^{hi} murine macrophages compared to MHC Class II^{hi} murine macrophages (Supplementary Table S2). Gene set enrichment analysis was performed using GSEA v_4.0.3. Gene sets obtained from Molecular Signatures Database c5.go.v2023.1.Hs.symbols.

Mice

C57BL/6J (B6), B6.129P2(Cg)-*Cx3cr1*$^{tm2.1(cre/ERT2)Litt}$/WganJ (Cx3cr1$^{CreERT2\text{-}YFP}$), B6.SJL-*Ptprc*^{a} *Pepc*^{b}/BoyJ (CD45.1^{+}), and B6.Cg-*Gt (ROSA)26Sor*$^{tm14(CAG\text{-}tdTomato)Hze}$/J (LSL-tdTomato) mice were purchased from the Jackson Laboratory and either used or bred in-house.

OMP-GFP on C57BL/6 background[61] mice were provided by Dorian McGavern (NINDS). B6.BAC.Cxcl9^{RFP}Cxcl10^{BFP} (REX3) mice[64] were provided by Andrew Luster (MGH/Harvard). Mice were bred and maintained under specific pathogen-free conditions at Duke University School of Medicine. Mice used in this study were between 6 and 26 weeks of age. Male and female mice were equally represented across experiments (no phenotypic differences between male and female mice were observed). All mice in this study were handled in accordance with the guidelines set forth by the Duke Animal Care and Use Committee.

Viruses

Vesicular stomatitis virus expressing ovalbumin, serotype Indiana virus (VSV) (provided by Dorian McGavern, NINDS) was propagated on Vero cells. Influenza B/Malaysia/2506/2004 virus (Mal/04) (originally provided by Nicholas Heaton, Duke) was grown in embryonated chicken eggs in a humidified incubator at 33 °C. Mice were infected intranasally (IN) by pipetting 10 μL of viral diluent in each nostril (1 x 10^5 PFU VSV or 3 x 10^6 PFU Mal/04) under anesthesia.

Immunohistochemistry

Mice were perfused intracardially with 2.5 % neutral buffered formalin (NBF) and skin around the head and nose was removed before fixing whole heads in 2.5 % NBF overnight at 4 °C. Heads were then submerged in a 0.5 M EDTA solution for 5–7 days at 4 °C to decalcify bone around the olfactory regions. Once decalcified, heads were embedded in tissue freezing medium (Triangle Biomedical Sciences) for sagittal or coronal sections. Cryosections were cut using a Leica CM1850 cryostat at a thickness of 30 μm after which sections were washed and stained in PBS. Primary antibodies were incubated on cryosections overnight at 4 °C. After staining, sections were washed 4–5 times with PBS, and 2–3 drops of Mowiol Mounting Media (9.6 % (w/v) Mowiol 4–88, 24 % (w/v) glycerol, 2.5 % DABCO, 0.1 M Tris-Cl pH 8.5 in water) were added to each section before addition of a coverslip.

For whole mount imaging of olfactory mucosa, tissue from the septum was dissected as previously described[60]. The tissue was submerged in PBS with the staining antibody for 1 h at room temperature before fixation with 2.5 % NBF for 3 h at room temperature. The olfactory tissue was sandwiched between two coverslips to enable confocal imaging of both sides of the tissue. Images were acquired using a Leica SP8 Upright Confocal Microscope equipped with 405 nm diode laser, Argon (458, 488, 514 nm) laser, 561 nm diode laser, and HeNe 633 nm laser. Image analysis was performed using Imaris software (Bitplane) version 7.6.1 using the surfaces function to define macrophage populations and associated statistics.

Flow cytometry and cell isolation

Olfactory mucosa and olfactory bulb samples were harvested from mice following intracardial perfusion with PBS as previously described[53]. Five minutes prior to sacrifice, 5 μL of α-CD45.2 antibody was pipetted into both nostrils of the mouse. Tissues were minced and digested in Hibernate A with DNase I (Roche, 0.5 mg/mL) and Collagenase D (Roche, 0.5 mg/mL) at 37° C for 30 min with constant shaking. Cells were washed, spun down at 500 x g for 5 min, and resuspended in PBS. Cells were blocked on ice for 20 min with Fc block (Biolegend #101301). Cells were then washed, spun down at 500 x g for 5 min, and stained with antibodies and Zombie UV Viability Dye (Biolegend #423107) on ice for 20 min. Antibodies used in this study include CD45-BUV395 (BD Horizon #564279), CD45.2-PacBlue (Biolegend #109820), CD11b-BUV797 (BD Horizon #564443), F4/80-APC-Fire750 (Biolegend #123151), CD64-PE-Cy7 (Biolegend #139313), P2ry12-APC (Biolegend #848006), MHC Class II IA/IE-BV785 (Biolegend #107645), Ly-6C-BV605 (Biolegend #128035). After a final wash and resuspension, counting beads (Precision Count Beads, Biolegend #424902) were added and samples were analyzed on a BD Fortessa-X20 Flow Cytometer equipped with five lasers (UV, 405, 466, 561, and 640 nm excitation). Data analysis was conducted in FlowJo 10.9.0.

Macrophage phagocytosis

Olfactory mucosa was harvested from OMP-GFP mice (CD45.2$^+$) and WT congenic mice (CD45.1$^+$), and the tissues were digested together in the same well. The frequency of CD45.1$^+$ cells internalizing GFP was taken as the "*in vitro*" phagocytosis rate, while the frequency of CD45.2$^+$ cells internalizing GFP was considered the overall phagocytosis rate. The average level of CD45.1$^+$ internalization was subtracted from the overall rate to calculate an "*in vivo*" measure of phagocytosis. Macrophage internalization images were obtained using an Imagestream Mark II Flow Cytometer, and quantification was performed on a conventional Fortessa X20 flow cytometer.

Phagocytosis of pHrodo red bioparticles (ThermoFisher, P35361) was performed by isolating OM cells as above and incubating the cells with the bioparticles for 20 min at 37 °C (or 4 °C as a control). After washing with PBS, cells were stained for flow cytometry as before, taking care to keep the cells at 4 °C for the remainder of the procedure.

Lineage tracing

Cx3cr1$^{CreERT2\text{-}YFP}$ x LSL-tdTomato mice were tamoxifen treated (2 mg/mouse, 3 doses across 5 days) at 6 weeks of age. Tissues were harvested every 4 weeks after tamoxifen treatment. Macrophages were gated on Cx3cr1^{YFP}+, CD11b+, F4/80 + and CD64 + . For post-infection lineage tracing, mice were VSV infected (10^5 PFU) intranasally 4 weeks after initial tamoxifen treatment.

Statistical analysis and graphics

All statistical analyses were performed in GraphPad Prism 10.1.0 as indicated in the figure legends. Plots were generated in Prism and original diagrams were created with BioRender.com.

Author contributions

SAW and EAM conceived the study and wrote the manuscript. EAM oversaw experimental design and execution of the project. SAW, CWC, KAB, EL, APM, and EAM performed experiments and interpreted data. MV, AS, JMO provided guidance, support, and performed experiments for scRNAseq analysis. All authors approve the final version of the manuscript.

CRediT authorship contribution statement

Sebastian A. Wellford: Writing – review & editing, Writing – original draft, Visualization, Validation, Methodology, Investigation, Formal analysis, Data curation, Conceptualization. **Ching-Wen Chen:** Methodology, Investigation. **Marko Vukovic:** Methodology, Investigation. **Kristen A. Batich:** Methodology, Investigation, Conceptualization. **Elliot Lin:** Investigation. **Alex K. Shalek:** Writing – review & editing, Supervision, Funding acquisition. **Jose Ordovas-Montanes:** Writing – review & editing, Supervision, Resources, Conceptualization. **Annie Park Moseman:** Writing – review & editing, Investigation. **E. Ashley Moseman:** Visualization, Investigation, Writing – review & editing, Supervision, Project administration, Investigation, Funding acquisition, Conceptualization.

Declaration of competing interest

The authors declare the following financial interests/personal relationships which may be considered as potential competing interests: [J.O.M. reports compensation for consulting services with Cellarity,

Tessel Biosciences, and Radera Biotherapeutics. A.K.S. reports compensation for consulting and/or SAB membership from Honeycomb Biotechnologies, Cellarity, Ochre Bio, Bio-Rad Laboratories, Relation Therapeutics, IntrECate biotherapeutics, Fog Pharma, Passkey Therapeutics, and Dahlia Biosciences unrelated to this work].

Acknowledgements

E.A.M is partially supported by R01NS121067, R21NS133561, and R21DC021260 and by a Duke School of Medicine Whitehead Family Scholarship. S.A.W received support from T32AI052077. J.O.M is a New York Stem Cell Foundation – Robertson Investigator. J.O.M was supported by the AbbVie-Harvard Medical School Alliance, The Pew Charitable Trusts Biomedical Scholars, The New York Stem Cell Foundation, NIH R01 HL162642 and The Cell Discovery Network, a collaborative funded by The Manton Foundation and The Warren Alpert Foundation at Boston Children's Hospital. A.K.S. was supported by the Searle Scholars Program the Beckman Young Investigator Program, NIH New Innovator Award DP2GM119419, and NIH U24 AI11862-01.

Appendix A. Supplementary data

Supplementary data to this article can be found online at https://doi.org/10.1016/j.mucimm.2024.07.009.

References

1. Lazarov T, Juarez-Carreño S, Cox N, Geissmann F. Physiology and diseases of tissue-resident macrophages. *Nature*. 2023;618(7966):698–707.
2. Mass E, Nimmerjahn F, Kierdorf K, Schlitzer A. Tissue-specific macrophages: how they develop and choreograph tissue biology. *Nat Rev Immunol*. 2023;23:563–579.
3. Nobs SP, Kopf M. Tissue-resident macrophages: guardians of organ homeostasis. *Trends Immunol*. 2021;42(6):495–507.
4. Zhao J, Andreev I, Silva HM. Resident tissue macrophages: Key coordinators of tissue homeostasis beyond immunity. *Sci Immunol*. 2024;9(94):eadd1967.
5. Chakarov S, Lim HY, Tan L, et al. Two distinct interstitial macrophage populations coexist across tissues in specific subtissular niches. *Science*. 2019;363(6432):eaau0964.
6. Blériot C, Chakarov S, Ginhoux F. Determinants of Resident Tissue Macrophage Identity and Function. *Immunity*. 2020;52(6):957–970.
7. Silvin A, Ginhoux F. Microglia heterogeneity along a spatio-temporal axis: More questions than answers. *Glia*. 2018;66(10):2045–2057.
8. Li Q, Barres BA. Microglia and macrophages in brain homeostasis and disease. *Nat Rev Immunol*. 2018;18(4):225–242.
9. Borst K, Dumas AA, Prinz M. Microglia: Immune and non-immune functions. *Immunity*. 2021;54(10):2194–2208.
10. Bennett ML, Bennett FC. The influence of environment and origin on brain resident macrophages and implications for therapy. *Nat Neurosci*. 2020;23:157–166.
11. Masuda T, Amann L, Monaco G, et al. Specification of CNS macrophage subsets occurs postnatally in defined niches. *Nature*. 2022;604(7907):740–748.
12. Sankowski R, Süß P, Benkendorff A, et al. Multiomic spatial landscape of innate immune cells at human central nervous system borders. *Nat Med*. 2024;30(1):186–198.
13. Da Mesquita S, Rua R. Brain border-associated macrophages: common denominators in infection, aging, and Alzheimer's disease? *Trends Immunol*. 2024 May;45(5):346–357.
14. Vlaminck KD, Hove HV, Kancheva D, et al. Differential plasticity and fate of brain-resident and recruited macrophages during the onset and resolution of neuroinflammation. *Immunity*. 2022;55(11):2085–2102.
15. Rebejac J, Eme-Scolan E, Paroutaud LA, et al. Meningeal macrophages protect against viral neuroinfection. *Immunity*. 2022;55(11):2103–2117.
16. Viola MF, Chavero-Pieres M, Modave E, et al. Dedicated macrophages organize and maintain the enteric nervous system. *Nature*. 2023;618:1–9.
17. Kolter J, Feuerstein R, Zeis P, et al. A Subset of Skin Macrophages Contributes to the Surveillance and Regeneration of Local Nerves. *Immunity*. 2019;50(6):1482–1497.e1487.
18. Ural BB, Yeung ST, Damani-Yokota P, et al. Identification of a nerve-associated, lung-resident interstitial macrophage subset with distinct localization and immunoregulatory properties. *Sci Immunol*. 2020;5(45):eaax8756.
19. Kolter J, Kierdorf K, Henneke P. Origin and Differentiation of Nerve-Associated Macrophages. *The Journal of Immunology*. 2020;204(2):271–279.
20. Wang PL, Yim AK, Kim K-W, et al. Peripheral nerve resident macrophages share tissue-specific programming and features of activated microglia. *Nat Commun*. 2020;11(1):2552.
21. Ydens E, Amann L, Asselbergh B, et al. Profiling peripheral nerve macrophages reveals two macrophage subsets with distinct localization, transcriptome and response to injury. *Nat Neurosci*. 2020;23:676–689.
22. Chen CR, Kachramanoglou C, Li D, Andrews P, Choi D. Anatomy and cellular constituents of the human olfactory mucosa: a review. *Journal of neurological surgery Part B, Skull base*. 2014;75(5):293–300.
23. Dando SJ, Mackay-Sim A, Norton R, et al. Pathogens penetrating the central nervous system: infection pathways and the cellular and molecular mechanisms of invasion. *Clin Microbiol Rev*. 2014;27(4):691–726.
24. Wellford SA, Moseman EA. Olfactory immunology: the missing piece in airway and CNS defence. *Nat Rev Immunol*. 2024;24:381–398.
25. Wellford SA, Moseman EA. Olfactory immune response to SARS-CoV-2. *Cell Mol Immunol*. 2024;21(2):134–143.
26. Seiden AM. Postviral olfactory loss. *Otolaryngol Clin North Am*. 2004;37(6):1159–1166.
27. Hura N, Xie DX, Choby GW, et al. Treatment of post-viral olfactory dysfunction: an evidence-based review with recommendations. *International Forum of Allergy & Rhinology*. 2020;10(9):1065–1086.
28. Meng X, Deng Y, Dai Z, Meng Z. COVID-19 and anosmia: A review based on up-to-date knowledge. *American Journal of Otolaryngology - Head and Neck Medicine and Surgery*. 2020;41(5):102581.
29. Narayanan SN, Shivappa P, Padiyath S, Bhaskar A, Li YW, Merghani TH. The Prevalence and Pathophysiology of Chemical Sense Disorder Caused by the Novel Coronavirus. *Front Public Health*. 2022;10, 839182.
30. Choi R, Goldstein BJ. Olfactory epithelium: Cells, clinical disorders, and insights from an adult stem cell niche. *Laryngoscope Investigative Otolaryngology*. 2018;3(1):35–42.
31. Mellert TK, Getchell ML, Sparks L, Getchell TV. Characterization of the immune barrier in human olfactory mucosa. *Otolaryngol Head Neck Surg*. 1992;106(2):181–188.
32. Getchell ML, Getchell TV. Immunohistochemical localization of components of the immune barrier in the olfactory mucosae of salamanders and rats. *Anat Rec*. 1991;231(3):358–374.
33. Smithson LJ, Kawaja MD. Microglial/macrophage cells in mammalian olfactory nerve fascicles. *J Neurosci Res*. 2010;88(4):858–865.
34. Borders AS, Getchell ML, Etscheidt JT, van Rooijen N, Cohen DA, Getchell TV. Macrophage depletion in the murine olfactory epithelium leads to increased neuronal death and decreased neurogenesis. *J Comp Neurol*. 2007;501(2):206–218.
35. Borders AS, Hersh MA, Getchell ML, et al. Macrophage-mediated neuroprotection and neurogenesis in the olfactory epithelium. *Physiol Genomics*. 2007;31(3):531–543.
36. Nan B, Getchell ML, Partin JV, Getchell TV. Leukemia inhibitory factor, interleukin-6, and their receptors are expressed transiently in the olfactory mucosa after target ablation. *J Comp Neurol*. 2001;435(1):60–77.
37. Getchell ML, Li H, Vaishnav RA, et al. Temporal gene expression profiles of target-ablated olfactory epithelium in mice with disrupted expression of scavenger receptor A: impact on macrophages. *Physiol Genomics*. 2006;27(3):245–263.
38. Getchell TV, Shah DS, Partin JV, Subhedar NK, Getchell ML. Leukemia inhibitory factor mRNA expression is upregulated in macrophages and olfactory receptor neurons after target ablation. *J Neurosci Res*. 2002;67(2):246–254.
39. Getchell TV, Subhedar NK, Shah DS, et al. Chemokine regulation of macrophage recruitment into the olfactory epithelium following target ablation: Involvement of macrophage inflammatory protein-1? and monocyte chemoattractant protein-1. *J Neurosci Res*. 2002;70(6):784–793.
40. Shi J, Li Z, Zhang J, et al. PHEV infection: A promising model of betacoronavirus-associated neurological and olfactory dysfunction. *PLoS Pathog*. 2022;18(6):e1010667.
41. Yoshida T, Nishiyama Y, Kimura Y, et al. Olfactory receptor neurons prevent dissemination of neurovirulent influenza A virus into the brain by undergoing virus-induced apoptosis. *J Gen Virol*. 2002;83(9):2109–2116.
42. Herbert RP, Harris J, Chong KP, Chapman J, West AK, Chuah MI. Cytokines and olfactory bulb microglia in response to bacterial challenge in the compromised primary olfactory pathway. *J Neuroinflammation*. 2012;9(1):109.
43. Chen M, Reed R. Chronic inflammation directs an olfactory stem cell functional switch from neuroregeneration to immune defense. *Cell Stem Cell*. 2019;25(4):501–513.
44. Kazer SW, Match CM, Langan EM, et al. Primary nasal viral infection rewires the tissue-scale memory response. *bioRxiv*. 2011;2023(2023).
45. Ruitenberg MJ, Vukovic J, Blomster L, et al. CX3CL1/fractalkine regulates branching and migration of monocyte-derived cells in the mouse olfactory epithelium. *J Neuroimmunol*. 2008;205(1–2):80–85.
46. Vukovic J, Blomster LV, Chinnery HR, et al. Bone marrow chimeric mice reveal a role for CX3CR1 in maintenance of the monocyte-derived cell population in the olfactory neuroepithelium. *J Leukoc Biol*. 2010;88(4):645–654.
47. Blomster LV, Vukovic J, Hendrickx DAE, et al. CX3CR1 deficiency exacerbates neuronal loss and impairs early regenerative responses in the target-ablated olfactory epithelium. *Mol Cell Neurosci*. 2011;48(3):236–245.
48. Reiss CS, Plakhov IV, Komatsu T. Viral Replication in Olfactory Receptor Neurons and Entry into the Olfactory Bulb and Brain. *Ann N Y Acad Sci*. 1998;855:751–761.
49. Ziegler CGK, Allon SJ, Nyquist SK, et al. SARS-CoV-2 Receptor ACE2 Is an Interferon-Stimulated Gene in Human Airway Epithelial Cells and Is Detected in Specific Cell Subsets across Tissues. *Cell*. 2020;181(5):1016–1035.e1019.
50. Ualiyeva S, Lemire E, Wong C, et al. A nasal cell atlas reveals heterogeneity of tuft cells and their role in directing olfactory stem cell proliferation. *Sci Immunol*. 2024;9(92):eabq4341.
51. Ginhoux F, Guilliams M. Tissue-Resident Macrophage Ontogeny and Homeostasis. *Immunity*. 2016;44(3):439–449.

52. Brioschi S, Belk JA, Peng V, et al. A Cre-deleter specific for embryo-derived brain macrophages reveals distinct features of microglia and border macrophages. *Immunity*. 2023;56(5):1027–1045.
53. Wellford SA, Moseman EA. Identification of Immune Cells in Murine Olfactory Mucosa. *The Olfactory System. Methods Mol Biol*. 2023;2710:61–69.
54. Madisen L, Zwingman TA, Sunkin SM, et al. A robust and high-throughput Cre reporting and characterization system for the whole mouse brain. *Nat Neurosci*. 2010;13(1):133–140.
55. Moseman EA, Blanchard AC, Nayak D, McGavern DB. T cell engagement of cross-presenting microglia protects the brain from a nasal virus infection. *Sci Immunol*. 2020;5(48):eabb1817.
56. Barrios AW, Nunez G, Sanchez Quinteiro P, Salazar I. Anatomy, histochemistry, and immunohistochemistry of the olfactory subsystems in mice. *Front Neuroanat*. 2014;8 (July):1–10.
57. Savage JC, Carrier M, Tremblay M-È. Morphology of microglia across contexts of health and disease. *Methods Mol Biol*. 2019;2034:13–26.
58. Gordon S, Plüddemann A, Martinez EF. Macrophage heterogeneity in tissues: phenotypic diversity and functions. *Immunol Rev*. 2014;262(1):36–55.
59. Vidal-Itriago A, Radford RAW, Aramideh JA, et al. Microglia morphophysiological diversity and its implications for the CNS. *Front Immunol*. 2022;13, 997786.
60. Oberland S, Neuhaus EM. Whole mount labeling of cilia in the main olfactory system of mice. *Journal of visualized experiments : JoVE*. 2014;94:52299.
61. Potter SM, Zheng C, Koos DS, Feinstein P, Fraser SE, Mombaerts P. Structure and emergence of specific olfactory glomeruli in the mouse. *J Neuroscience*. 2001;21(24): 9713–9723.
62. Szabo-Pardi TA, Syed UM, Castillo ZW, Burton MD. Use of integrated optical clearing and 2-photon imaging to investigate sex differences in neuroimmune interactions after peripheral nerve injury. *Front Cell Dev Biol*. 2021;9, 624201.
63. Dumm RE, Wellford SA, Moseman EA, Heaton NS. Heterogeneity of Antiviral Responses in the Upper Respiratory Tract Mediates Differential Non-lytic Clearance of Influenza Viruses. *Cell Rep*. 2020;32(9):108103.
64. Groom JR, Richmond J, Murooka TT, et al. CXCR3 chemokine receptor-ligand interactions in the lymph node optimize CD4+ T helper 1 cell differentiation. *Immunity*. 2012;37(6):1091–1103.
65. Sung JH, Zhang H, Moseman EA, et al. Chemokine guidance of central memory T cells is critical for antiviral recall responses in lymph nodes. *Cell*. 2012;150(6): 1249–1263.
66. Finlay JB, Brann DH, Abi Hachem R, et al. Persistent post-COVID-19 smell loss is associated with immune cell infiltration and altered gene expression in olfactory epithelium. *Sci Transl Med*. 2022;14(676):eadd0484.
67. Schyns J, Bai Q, Ruscitti C, et al. Non-classical tissue monocytes and two functionally distinct populations of interstitial macrophages populate the mouse lung. *Nat Commun*. 2019;10(1):3964.
68. Buttgereit A, Lelios I, Yu X, et al. Sall1 is a transcriptional regulator defining microglia identity and function. *Nat Immunol*. 2016;17(12):1397–1406.
69. McKinsey GL, Lizama CO, Keown-Lang AE, et al. A new genetic strategy for targeting microglia in development and disease. *Elife*. 2020;9:e54590.
70. Cserép C, Pósfai B, Lénárt N, et al. Microglia monitor and protect neuronal function via specialized somatic purinergic junctions. *Science*. 2019;367(6477):eaax6752.
71. Huang Y, Happonen KE, Burrola PG, et al. Microglia use TAM receptors to detect and engulf amyloid β plaques. *Nat Immunol*. 2021;22(5):586–594.
72. Lampinen R, Fazaludeen MF, Avesani S, et al. Single-Cell RNA-Seq Analysis of Olfactory Mucosal Cells of Alzheimer's Disease Patients. *Cells*. 2022;11(4):676.
73. Kreisl WC, Jin P, Lee S, et al. Odor identification ability predicts PET amyloid status and memory decline in older adults. *J Alzheimers Dis*. 2018;62(4):1759–1766.
74. Eyo U, Molofsky AV. Defining microglial-synapse interactions. *Science*. 2023;381 (6663):1155–1156.
75. Wang C, Yue H, Hu Z, et al. Microglia mediate forgetting via complement-dependent synaptic elimination. *Science*. 2020;367(6478):688–694.
76. Berglund R, Guerreiro-Cacais AO, Adzemovic MZ, et al. Microglial autophagy–associated phagocytosis is essential for recovery from neuroinflammation. *Sci Immunol*. 2020;5(52):eabb5077.
77. Podleśny-Drabiniok A, Marcora E, Goate AM. Microglial Phagocytosis: A Disease-Associated Process Emerging from Alzheimer's Disease Genetics. *Trends Neurosci*. 2020;43(12):965–979.
78. Oliva AD, Gupta R, Issa K, et al. Aging-related olfactory loss is associated with olfactory stem cell transcriptional alterations in humans. *J Clin Invest*. 2022;132(4).
79. Wellford SA, Moseman AP, Dao K, et al. Mucosal plasma cells are required to protect the upper airway and brain from infection. *Immunity*. 2022;55(11):2118–2134.
80. Ronaldson PT, Davis TP. Regulation of blood–brain barrier integrity by microglia in health and disease: A therapeutic opportunity. *J Cereb Blood Flow Metab*. 2020;40: S6–S24.
81. Bisht K, Okojie KA, Sharma K, et al. Capillary-associated microglia regulate vascular structure and function through PANX1-P2RY12 coupling in mice. *Nat Commun*. 2021;12(1):5289.
82. Erblich B, Zhu L, Etgen AM, Dobrenis K, Pollard JW. Absence of Colony Stimulation Factor-1 Receptor Results in Loss of Microglia, Disrupted Brain Development and Olfactory Deficits. *PLoS One*. 2011;6(10):e26317–e.
83. Sariol A, Mackin S, Allred M-G, et al. Microglia depletion exacerbates demyelination and impairs remyelination in a neurotropic coronavirus infection. *Proc Natl Acad Sci*. 2020:202007814.
84. Qi L, Li X, Zhang F, et al. VEGFR-3 signaling restrains the neuron-macrophage crosstalk during neurotropic viral infection. *Cell Rep*. 2023;42(5), 112489.
85. Kim Y-C, Ahn JH, Jin H, et al. Immaturity of immune cells around the dural venous sinuses contributes to viral meningoencephalitis in neonates. *Sci Immunol*. 2023;8 (88):eadg6155.
86. Loske J, Röhmel J, Lukassen S, et al. Pre-activated antiviral innate immunity in the upper airways controls early SARS-CoV-2 infection in children. *Nat Biotechnol*. 2022 Mar;40(3):319–324.
87. Finlay JB, Brann DH, Abi Hachem R, et al. Persistent post–COVID-19 smell loss is associated with immune cell infiltration and altered gene expression in olfactory epithelium. *Sci Transl Med*. 2022;14(676):eadd0484.
88. Gierahn TM, Wadsworth MH, Hughes TK, et al. Seq-Well: portable, low-cost RNA sequencing of single cells at high throughput. *Nat Methods*. 2017;14(4):395–398.